Differentiating tumor heterogeneity in FFPE prostate adenocarcinoma tissues using PCA analysis of MALDI IMS spectral data

Irene Panderi*[1,2], Evgeny Yakirevich[3], Silvana Papagerakis[4], Lelia Noble[1], Kara Lombardo[3], Dionysios Pantazatos[1,5]

[1] Brown University, Warren Alpert Medical School, COBRE Center for Cancer Research, Rhode Island Hospital, Providence, RI, USA

[2] National and Kapodistrian University of Athens, Department of Pharmacy, Division of Pharmaceutical Chemistry, Laboratory of Pharmaceutical Analysis, Athens, Greece

[3] Brown University, Warren Alpert Medical School, Department of Pathology, Rhode Island Hospital, Providence, RI, USA

[4] University of Michigan Comprehensive Cancer Center, School of Medicine, Department of Periodontics and Oral Medicine, Division of Oral Pathology/Medicine/Radiology, Ann Arbor MI

[5] Weill Cornell Medical College, Division of Infectious Diseases, Transplantation-Oncology Infectious Disease Program, New York, NY, USA

This is the author manuscript accepted for publication and has undergone full peer review but has not been through the copyediting, typesetting, pagination and proofreading process, which may lead to differences between this version and the Version of Record. Please cite this article as doi: 10.1002/rcm.7776

* Correspondence to Irene Panderi, National and Kapodistrian University of Athens, Department of Pharmacy, Division of Pharmaceutical Chemistry, Laboratory of Pharmaceutical Analysis, Panepistimiopolis, Zografou 15771, Athens-Greece, e-mail: irenepanderi@gmail.com, Tel.: +30-6974015798

ABSTRACT

RATIONALE: Many patients with adenocarcinoma of the prostate present with advanced and metastatic cancer at the time of diagnosis. There is an urgent need to detect biomarkers that will improve the diagnosis and prognosis of this disease. MALDI imaging mass spectrometry (MALDI-IMS) is playing a key role in cancer research and it can be useful to unravel the molecular profile of prostate cancer biopsies.

METHODS: MALDI imaging data sets are highly complex and their interpretation requires the use of multivariate statistical methods. In this study MALDI-IMS technology, sequential principal component analysis (PCA) and 2-D peak distribution tests were employed to investigate tumor heterogeneity in formalin-fixed paraffin-embedded (FFPE) prostate cancer biopsies.

RESULTS: Multivariate statistics revealed a number of mass ion peaks obtained from different tumor regions that were distinguishable from the adjacent normal regions within a given specimen. These ion peaks have been used to generate ion images and visualize the difference between tumor and normal regions. Mass peaks at m/z 3370, 3441, 3447 and 3707 exhibited stronger ion signals in the tumor regions.

CONCLUSIONS: This study reports statistically significant mass ion peaks unique to tumor regions in adenocarcinoma of the prostate and adds to the clinical utility of MALDI-IMS for analysis of FFPE tissue at a molecular level that supersedes all other standard histopathologic techniques for diagnostic purposes used in the current clinical practice.

KEYWORDS: MALDI IMS, Prostate cancer, Principal Component Analysis, Formalin-fixed paraffin-embedded tissues.

INTRODUCTION

Since its inception twenty years ago, matrix-assisted laser desorption/ionization mass spectrometry imaging (MALDI-IMS) has matured as a powerful tool that provides new insight into molecular physiopathology of diseases [1-3]. The technique is widely used in biomedical research for profiling the distribution of proteins, peptides, and small molecules on tissue [4-6]. In addition, MALDI-IMS provides reproducible high-resolution mass measurements of molecules in complex biological matrices such as cells and serum samples [7, 8]. MALDI IMS plays a key role in the discovery of biomarkers for the diagnosis of cancer and classification of the disease pathology [9, 10]. Given its ability to localize proteins and smaller molecules across an entire tissue section, MALDI-IMS analysis holds promise in the elucidation of molecular processes in the tumor microenvironment [11].

Comprehensive visualization of distribution of biomolecules across tissue sections by defining peptide ions specific for various tumor regions may improve the classification and prognosis of cancer [12-14]. In this paper we describe the use of sequential principal component analysis (PCA) of MALDI IMS data sets to unveil the

molecular profile in formalin-fixed paraffin-embedded (FFPE) tissues of adenocarcinoma of the prostate. Adenocarcinoma of the prostate is the most common type of prostate cancer (PCa) [15,16]. However, it is a type of cancer with a wide range of behavior from cases which are very slow growing to cases which are more aggressive and many patients present with advanced and metastatic cancer at the time of diagnosis [17]. Thus, there is an urgent need to identify biomarkers that will improve the diagnosis and prognosis of this disease [18]. The ability of MALDI-IMS to localize molecular changes within a tissue section at a cellular level and to allow for accurate positive, differential and exclusion diagnosis of a given disease, can significantly improve the diagnosis of PCa [19]. A number of studies have been carried out to search for biomarkers for PCa diagnosis in various biomaterials [20-22]. Recently, MALDI MS profiling of serum proteins demonstrated the ability to discriminate PCa patients' profiles from control samples [23]. MALDI-TOF-MS protein profiles of urine samples of healthy donors have been compared to prostate cancer patients for a differential proteomic study [24]. Matrix coating assisted by an electric field (MCAEF) has been used for overall enhancement of MALDI-IMS of human prostate cancer biomarkers [25]. However, only a limited number of studies were performed at a molecular level using MALDI IMS for a direct tissue correlated proteome analysis [26]. Some potential PCa biomarkers have been reported using MALDI-IMS analysis of fresh-frozen prostate cancer tissues [27-32]. The major disadvantage of using fresh-frozen tissues is the limited availability of tissues for which clinical follow-up data are available. The major source of tissue samples are

FFPE tissues found in hospital archives and their use helps to alleviate many of the problems associated with frozen tissues [33]. In addition, FFPE tissues are much easier to store and transport because they are stable at room temperature so methods and technologies that permit analysis of large numbers of such samples are essential [34]. Several protocols of heat induced antigen retrieval (HIAR) procedures have previously been established that allow MALDI-IMS studies in various FFPE tissue types [35-37]. However, it is currently well known that although these protocols are applicable to many tissue types, to achieve optimal results, the HIAR procedure for each different tissue type should be optimized [38,39]. Recently, tissue microarray technology in combination with MALDI-IMS operated in positive reflectron mode over the mass per charge (m/z) range of 500–3,680 has been employed to identify molecular features associated with clinico-pathological parameters in FFPE prostate cancer tissues [40]. Given this development the employment of a MALDI-IMS method in positive linear mode over the mass per charge (m/z) range of 2,000-20,000 to analyze FFPE prostate tissue biopsies would be of great clinical value.

To the best of our knowledge it is the first time that a multivariate statistical approach based on sequential PCA analysis is proposed for a direct tissue correlated proteome analysis of FFPE prostate cancer biopsies using MALDI IMS. In this study FFPE samples were processed using a HIAR procedure to restore normal protein composition and increase the signal and the number of mass ion peaks detected with MALDI-IMS. Due to the high complexity of MALDI imaging data sets their interpretation requires the use of multivariate statistical methods to reduce data

dimensionality and determine the components that correlate to the and classification of the data [41-44]. Therefore data analysis in this study was performed using sequential PCA so as to identify and classify the ion peaks that allowed the accurate differentiation of samples. PCA carries out linear orthogonal transformation of the data to maximize variance, resulting in a set of orthogonal principal components that describe the largest variance in the dataset [45-47]. The results underline the vast potential of MALDI-IMS in combination with principal component analysis to detect molecular patterns suitable to distinguish between tumor and normal prostate tissues. These specific and statistically significant ion peaks may serve as potential biomarkers for adenocarcinoma of the prostate in FFPE tissue section samples.

MATERIALS AND METHODS

Materials

All solvents used were of HPLC grade and purchased from E. Merck (Darmstadt, Germany). Xylene was of analytical reagent grade and purchased from J.T. Baker (Phillipsburg, NJ). Conductive indium tin oxide (ITO) one-site coated glass slides and peptide calibration standard II were purchased from Bruker Daltonik GmbH (Billerica, MA). Sinapinic acid (SA) was purchased from Sigma-Aldrich (St Louis, MO).

Sample collection

Prostate tissues were collected with the consent of patients undergoing surgery at the Rhode Island Hospital in Providence, RI. In this pilot study, FFPE tissues of two patients (case 1 and case 2) with adenocarcinoma of the prostate were used. Normal areas were also used as reference controls. The tissue samples were removed by surgery according to the standard local therapeutic protocol. Pathological appearances of the tissue samples were microscopically determined by an experienced pathologist.

Sample preparation

FFPE samples were fixed in 10% buffered formalin for 24 h, at room temperature, dehydrated with ethanol and paraffin-embedded according to the standard local protocol. The samples were cut into 4μm tissue sections using a Leica RM2125RT microtome operated at room temperature and applied onto ITO one-side coated, conductive glass slides. Each slide contained one tumor and one normal section. The samples were dried under vacuum for 30 min and then kept at 37^{o}C overnight to facilitate adhesion of the section to the target. The paraffin was removed with xylene washes twice for 3 min each before hydration with graded ethanol washes (100% ethanol for 2 min, 95% ethanol for 2 min and 70% ethanol for 1 min) and then rinsed with distilled water three times for 2 min each. After fully drying for one hour in an oven at 65^{o}C, the samples were immerged into a pre-heated steamer containing either TRIS buffer pH 9 or citrate buffer pH 6 at 95^{o}C for 55 min. After cooling at room temperature for 20 minutes the samples were rinsed with distilled water three times

for 5 min each. The samples were then dried under vacuum for 30 min before matrix application.

Matrix application

The Image Prep (Bruker Daltonics) was used for matrix application of 10 mg/mL sinapinic acid in acetonitrile/water 60/40 v/v containing 0.2 % trifluoroacetic acid. Spraying was accomplished using the ImagePrep standard programs.

MALDI imaging mass spectrometry

Spectra were collected across selected tissue areas using the Ultraflex III MALDI-TOF/TOF instrument (Bruker Daltonics) with a SmartBeam laser operating at 100 Hz in positive linear mode over the mass per charge (m/z) range of 2,000 to 20,000. A laser spot diameter of 100 μm and a raster width of 100 μm were used. Using the FlexImaging software (Bruker Daltonics), orientation points were generated to ensure the correct positioning of the laser for spectral acquisition. The software exported the specific geometry of the tissue to be analyzed, and an instrument-specific automated method was created, which generates a grid across the tissue of spots upon which data were acquired. Calibration was done externally using a protein standard mixture in the mass per charge range (m/z) of 3,000 to 16,500. The intensity of each scan, over the entire mass range acquired, was mapped on to the tissue section image, allowing the visualization of the location of each m/z detected. These images were generated and visualized using FlexImaging software. Consequently, the spectra derived from

regions of interest (ROIs) were exported for profile analysis. Normalizing, baseline subtracting, peak defining and comparison of multiple spectra were performed using ClinProtTools software. PCA and 2-D peak distribution were managed by an external MATLAB software tool, which was integrated in ClinProTools.

RESULTS AND DISCUSSION

MALDI-IMS analysis

FFPE tissue samples obtained from two prostate adenocarcinoma cancer patients were analyzed using MALDI-IMS and data were compared to match normal tissues stored under the same fixation procedure. The samples were processed using HIAR procedure using either TRIS buffer pH 9 or citrate buffer pH 6. FlexAnalysis software was used to compare the different MS spectra macroscopically. The spectra were then imported into the ClinProTools software for post-processing and generation of proteomic profiles. A resolution of 800 was applied to the peak detection method. The Convex Hull baseline with a flatness value of 0.8 was selected for baseline subtraction. Savitsky Golay algorithm was applied with a width of 2 m/z in 5 cycles for spectral smoothing. Null spectra exclusion filter was enabled with a noise threshold of 2, to exclude spectra with no data or extremely low intensities. Mass recalibration was not performed. A schematic experimental workflow is provided in Figure 1.

Statistical analysis of MALDI-IMS spectra

MALDI IMS spectra obtained from FFPE tissue sections were submitted to PCA analysis and 2-D distribution tests to identify mass peaks that differentiate between normal and tumor tissue sections. Each tumor and normal (non-tumor) tissue section was split into different regions of interest (ROIs). The total spectra of these ROIs were then exported to ClinProTools software for PCA analysis and 2-D distribution tests. PCA analysis calculated the variances between tumor, the adjacent normal regions within a given specimen and normal tissue sections. Multivariate analysis of the spectral data was repeated in both of the analyzed cases (Case 1 and Case 2) using either citrate buffer at pH 6 or TRIS buffer at pH 9 for the HIAR procedure.

Ion images of tumor and normal tissue sections of prostate tissue (Case 1) are presented in Figure 2A with highlighted the ROIs that were used to perform PCA analysis and 2-D distribution tests. PCA analysis revealed a series of significant ion peaks that account for the variation between tumor and normal ROIs. Score and loading outputs obtained from PCA analysis of tumor ROIs (T1 to T5) are presented in Fig. 2B. The score outputs demonstrated distinction between tumor ROIs T3 and T4 and ROIs T1, T2 and T5 in the three principal component (PC) coordinates. This distinction is also revealed in 2-D peak distribution plot presented in Figure 2C. PCA analysis was able to determine peaks that differentiated tumor ROIs T3 and T4 from normal ROIs (N1 to N4) and ROI T5 as it is illustrated in the score and loading outputs presented in Figure 2D and the 2-D distribution diagrams presented in Figure 2E. PCA analysis between tumor ROIs T1, T2, T3 and T4 (Fig. 2F) discriminated ROIs T3 and T4. This distinction is also illustrated in the 2-D peak distribution

diagram presented in Figure 2G. Average mass spectra of the selected ROIs and pseudo-gel view of mass ion peaks obtained from PCA analysis, all in the mass range 3 to 15 kDa, are presented in Figures 3A and 3B, respectively. Several mass ion peaks demonstrated distinction between tumor and normal ROIs and revealed the heterogeneity of tumor tissue sections. In particular, mass ion peaks at m/z 3369.8, 3440.7, 3484.7, 3707.9, 3719.2 and 13880.6 were overexpressed in tumor ROIs T3 and T4, mass ion peaks at m/z 3455.1, 4027.3 6283.1, 6643.4, 6656.2 and 6997.2 were more evident in ROIs T1 and T2 indicating tumor heterogeneity, while mass ion peaks at m/z 6013.1 and 6017.8 were overexpressed in normal ROIs. Tumor ROIs T3 and T4 have been further combined in one class using ClinProtSpectra import XML generator and compared to normal ROIs. A series of mass ion peaks that account for the variation between normal and tumor FFPE tissue sections can be observed in Figure 4a where the average mass spectra of tumor and normal ROIs, in the mass range 3 to 15 kDa, are presented. This distinction between tumor and normal ROIs is further revealed in a 3-D PCA plot and a 3-D peak distribution diagram presented in Figures 4B and 4C, respectively. Arrows in 3-D loading plots presented in Figure 4C indicate the placement of mass ion peak at m/z 3707 which is overexpressed in tumor regions and the placement of mass ion peak at m/z 4476 which is more evident in normal regions. Multivariate data analysis was repeated, as described above, in both FFPE cases studied. PCA of the spectral data revealed a series of significant ion peaks that account for the variation between tumor and normal tissue. Differentially expressed ion peaks have been ranked according to their signal to noise ratio using p-

value t-test ANOVA (Table 1). Mass ion peaks with m/z values of 3370, 3441, 3477, 5999, 6013, 6028, 6272, 6643, 6656, 6684, 6698 and 6799 appeared in both FFPE cases and independently of the buffer used for the HIAR procedure. The ion peaks with p-values less than 0.05 have been used to generate ion images and visualize the difference between tumor and normal ROIs. Among these molecular images, mass ion peaks at m/z 3370, 3441, 3447 and 3707 were detected to have stronger ion signals within tumor ROIs and could be used to distinguish prostate cancer tissue from normal prostate tissue.

Figure 5 illustrates MALDI ion images of tumor and normal FFPE tissue sections of case 1 processed with TRIS buffer pH 9 for the HIAR procedure using these distinct mass ion peaks. The spatial distribution of each of these ion peaks illustrated significant changes in intensity and varying distribution patterns among the different ROIs. Average mass spectra of tumor and normal ROIs in case 2 processed in citrate buffer pH 6 were in the mass per charge range (m/z) of 3 to 15 kDa along and MALDI ion images of the selected mass ion peaks that differentiate between normal and tumor tissue sections at m/z 3370, 3441, 3471, 4836, 6013 and 6272 are presented in Figure 6.

Our findings are in accordance with some of the MALDI IMS data presented in other studies. In MALDI MS profiling of human serum samples Fania and coworkers recently found an overexpression of the ion peaks at m/z 3448.63 and 6809.47 when compared with matched normal samples, which correlates with the ion peaks at m/z 3441 and 6799 detected in our study [23]. The mass ion peak at m/z 3441 was also

detected with increased expression in cancerous regions of fresh frozen prostate tissues in a MALDI IMS study presented by Schwamborn and coworkers [28]. In the latter study one other ion peak at m/z 4747 showed a slight overexpression in the cancerous regions, which agrees with the ion peak at m/z 4836 found in the FFPE prostate tissues analyzed in this work. Calvano and coworkers found that the MALDI MS signal intensity at m/z 6290 was higher for PCa urine samples when compared to healthy individuals, which agrees with the ion peak at m/z 6272 found in our study [24]. MALDI IMS analysis of fresh frozen tissues by Klocker and coworkers identified characteristic mass ion peaks that are able to discriminate between cancer, non-malignant benign epithelium and stromal areas ROIs [31]. In particular, mass ions peaks at m/z 4468, 6266 6284 and 6658 showed discriminatory ability to separate tumor areas versus benign epithelial non-malignant areas, a mass ion peak at m/z 3440 was also detected with increased expression in cancerous regions versus stromal areas and mass ion peaks at m/z 6284 and 6658 are discriminant for tumor versus stromal ROIs. The mass ion peak at m/z 6658 was identified in the same paper as biliverdin reductase B (BLVRB). BLVR subtype B is the major heme catabolizing enzyme during early fetal development and BLVR subtype A the major form of BLVR in the adult human liver [48]. In our study mass ion peaks at m/z 3441, 4476, 6271, 6283 and 6656 were also identified as discriminant peaks between tumor and normal ROIs of FFPE tissue sections which indicates that the proposed method can reveal the proteomic profile of prostate tissues and that the sequential PCA analysis used in this work is able to easily detect possible biomarkers for PCa. However, it

should be noted that mass differences between publications can be either explained by pre-analytical molecular changes, low-quality data acquisition, different biological matrix used for the analysis or closely related quasi molecular ions due to reactions during sample preparation, adduct ion formation or the loss of smaller functional groups [26].

CONCLUSION

The findings of this study demonstrate that multivariate analysis of MALDI IMS spectral data revealed a series of mass ion peaks that allowed the visualization of tumor ROIs and more importantly the ability to differentiate between tumor and normal ROIs in FFPE prostate tissue biopsies. Furthermore, PCA was able to differentiate specific mass ion peaks from different tumor regions within the same tissue defining the presence of tissue heterogeneity in FFPE prostate cancer specimens. The identification of the mass ion peaks responsible for the tissue heterogeneity within a prostate cancer specimen is of potential therapeutic interest and might play a key role to the understanding of the etiology of the disease. These mass ion peaks are probably a result of the molecular differences between different states of the disease.

The results highlight the degree of tumor heterogeneity inherent in prostate cancer biopsies. However, MALDI-IMS technology is challenging to directly detect high molecular mass biomarkers, with molecular mass greater than 25 kDa, that are currently used in clinical cancer research [49]. Therefore, the mass ion peaks detected in this pilot study represent low molecular weight biomolecules that can be fragments

of peptides or proteins which are up-regulated in prostate cancer and may play a role in signaling pathways of this disease. The detected mass ion peaks can differentiate between the tumor and normal regions and their identification may provide insight into new important therapeutic targets. This study provides evidence in support of the clinical utility of MALDI IMS which is able to annotate tissues based solely on the detected MS profiles and thereby differentiate regions that are not distinct using established histopathological tools but which are characterized by different MS signatures. This ability to effectively define tumor regions by molecular profiling at high resolution will provide a greater understanding of molecular mechanisms of tumor heterogeneity and warrants further studies for the identification of the most significant peaks. Furthermore, enrollment of a larger patient group will allow a better comparison of clinical and histopathological data using MALDI-IMS.

ACKNOWLEDMENTS

We would like to thank Dr. Paul Kowalski from Bruker Daltonics, Inc. USA for his support and help throughout this work.

FIGURE LEGENDS

Figure 1. Experimental workflow for imaging biomolecules in prostate cancer FFPE tissues.

Figure 2. A) MALDI ion images of normal and tumor sections of FFPE case 1 for m/z 3441 and 6012 showing the selected ROIs. PCA score and loading plots of tumor and normal ROIs (B, D, F) with their analogous 2-D distribution plots (C, E, G). Non-tumor ROIs N1 to N4 (blue), tumor ROIs T1 (bright green), T2 (dark green), T3 (red), T4 (brown), and T5 (pink).

Figure 3. A) Average mass spectra of FFPE case 1 processed with TRIS buffer pH 9 B). Pseudo-gel views of tumor ROIs T1 to T5 and normal ROIs N1 and N2 the x-axis indicates m/z mass value and y-axis is the spectra number used to produce the average mass value. Peak intensities are indicated as arbitrary units in the right intensity gradient.

Figure 4. A. Average mass spectra of the tumor (red) and normal (blue) ROIs of FFPE case 1 processed with TRIS buffer pH 9, in the mass to charge (m/z) range of 3 - 15 kDa. B. 3-D PCA plot, C. 2-D peak distribution diagram. Specific tumor (4476.4 m/z) and normal (3707 m/z) mass ion peaks in the mass spectra that participate in the differentiating class of peaks are indicated by red and blue arrows.

Figure 5. MALDI ion images of tumor and normal sections obtained from FFPE case 1 processed with TRIS buffer pH 9. Distribution of selected ion peaks demonstrate the ion peaks with m/z ratios 3370, 3707, 3441 and 3447 were localized on the same areas of the tumor tissue.

Figure 6. MALDI ion images of tumor and normal sections obtained from FFPE case 2 processed with TRIS buffer pH 6. Average mass spectra of the tumor (red) and normal (blue) ROIs of FFPE case 2 processed with citrate buffer pH 6, in the mass to charge (m/z) range of 3 - 15 kDa.

References

1. A. Bodzon-Kulakowska, P. Suder. Imaging mass spectrometry: Instrumentation, applications, and combination with other visualization techniques *Mass Spectrom Rev* **2016**, *35*, 147.
2. S.-R. Fagerer, A. Römpp, K. Jefimovs, R. Brönnimann, G. Hayenga, R.-F. Steinhoff, J. Krismer, M. Pabst, A.-J. Ibáñez, R. Zenobi. Resolution pattern for mass spectrometry imaging. *Rapid Commun Mass Spectrom.* **2015**, *29*, 1019.
3. J.-D.Watrous, T. Alexandrov, P.-C. Dorrestein, The evolving field of imaging mass spectrometry and its impact on future biological research. *J Mass Spectrom.* **2011**, *46*, 209.
4. S. Khatib-Shahidi, M. Andersson, J.-L. Herman, T.-A. Gillespie, R.-M. Caprioli. Direct molecular analysis of whole-body animal tissue sections by imaging MALDI mass spectrometry. *Anal. Chem.* **2006**, *78(18)*, 6448.
5. L. Guo, I. Panderi, D.-D. Yan, K. Szulak, Y. Li, Y.-T. Chen, H. Ma, D.-B. Niesen, N. Seeram, A. Ahmed, B. Yan, D. Pantazatos, W. Lu. A Comparative Study of Hollow Copper Sulfide Nanoparticles and Hollow Gold Nanospheres on Degradability and Toxicity. *ACS Nano* **2013**, *7(10)*, 8780.
6. R.-F. Menger, W.-L. Stutts, D.-S. Anbukumar, J.-A. Bowden, D.-A. Ford, R.-A. Yost. MALDI mass spectrometric imaging of cardiac tissue following myocardial infarction in a rat coronary artery ligation model. *Anal. Chem.* **2012**, *84 (2)*, 1117-1125.

7. S. Angeletti, G. Dicuonzo, A. Lo Presti, E. Cella, F. Crea, A. Avola, M. Andrea Vitali, M. Fagioni, L. De Florio. MALDI-TOF mass spectrometry and blakpc gene phylogenetic analysis of an outbreak of carbapenem-resistant K. pneumoniae strains. *New Microbiol* **2015**, *38*, 541.
8. C.-L. Gatlin, K.-Y. White, M.-B. Tracy, C.-E. Wilkins, O.-J. Semmes, J.O. Nyalwidh, R.R. Drake, D.I. Malyarenko. Enhancement in MALDI-TOF MS analysis of the low molecular weight human serum proteome. *J Mass Spectrom* **2011**, *46(1)*, 85.
9. C. Marquardt, T. Tolstik, C. Bielecki, R. Kaufmann, A.-C. Crecelius, U.-S. Schubert, U. Settmacher, A. Stallmach, O.-Z. Dirsch. MALDI imaging-based classification of hepatocellular carcinoma and non-malignant lesions in fibrotic liver tissue. *Gastroenterol* **2015**, *53*, 33.
10. M.-A.M. Rodrigo, O. Zitka, S. Krizkov, A. Moulick, V. Adam, R. Kizek. MALDI-TOF MS as evolving cancer diagnostic tool: A review. *J Pharm Biomed Anal* **2014**, *95*, 245.
11. E.-H. Seeley, R.-M. Caprioli. MALDI imaging mass spectrometry of human tissue: method challenges and clinical perspectives. *Trends Biotechnol* **2011**, *29(3)*, 136.
12. L.-A. McDonnell, G.-L. Corthals, S.-M. Willems, A. van Remoortere, R.J. van Zeijl, A.-M. Deelder. Peptide and protein imaging mass spectrometry in cancer research. *J. Proteome* **2010**, *73*, 1921.
13. S.-R. Oppenheimer, D. Mi, M.-E. Sanders, R.-M. Caprioli. A Molecular Analysis of Tumor Margins by MALDI Mass Spectrometry in Renal Carcinoma. *J Proteome Res* **2010**, *9(5)*, 2182.
14. R.- J.A. Goodwin, S.-R. Pennington, A.-R. Pitt. Protein and peptides in pictures: Imaging with MALDI mass spectrometry. *Proteomics* **2008,** *8*, 3785.
15. R.-L. Siegel, K.-D. Miller, A. Jemal. Cancer statistics. *Ca Cancer J Clin* **2016**, *66*, 7.
16. J. Ferlay, E. Steliarova-Foucher, J. Lortet-Tieulent, S. Rosso, J.-W.W. Coebergh, H. Comber, D. Forman, F. Bray. Cancer incidence and mortality

patterns in Europe: Estimates for 40 countries in 2012. *Eur J Canc* **2013**, *49*, 1374.

17. C.-A. Evans, A. Glen, C.-L. Eaton, S. Larré, J.-W.F. Catto, F.-C. Hamdy, P.-C. Wright, I. Rehman. Prostate cancer proteomics: The urgent need for clinically validated biomarkers. *Proteomics Clin Appl* **2009**, *3*, 197.
18. J.-C. Byrne, M.-R. Downes, N. O'Donoghue, C. O'Keane, A. O'Neill, Y. Fan, J.-M. Fitzpatrick, M. Dunn, R.-W. Watson. 2D-DIGE as a strategy to identify serum markers for the progression of prostate cancer. *J Proteome Res* **2009**, *8*, 942.
19. J.-O.R. Gustafsson, M.-K. Oehler, A. Ruszkiewicz , S.-R. McColl, P. Hoffmann. MALDI Imaging Mass Spectrometry (MALDI-IMS)-Application of Spatial Proteomics for Ovarian Cancer Classification and Diagnosis. *Int J Mol Sci* **2011**, *12(1)*, 773.
20. Z. Xiao, B.-L. Adam, L.-H. Cazares, M.-A. Clements, J.-W. Davis, P.-F. Schellhammer, E.-A. Dalmasso, G.-L. Wright. Quantitation of serum prostate-specific membrane antigen by a novel protein biochip immunoassay discriminates benign from malignant prostate disease. *Cancer Res* **2001**, *61*, 6029.
21. L.-J.M. Dekker, P.-C. Burgers, H. Charif, A.-L.C.T. van Rijswijk, M.-K. Titulaer, G. Jenster, R. Bischoff, C.-H. Bangma, T.-M. Luider. Differential expression of protease activity in serum samples of prostate carcinoma patients with metastases. *Proteomics* **2010**, *10*, 2348.
22. J.A. Al-Ruwaili, S.E. Larkin, B.A. Zeidan, M.G. Taylor, C.N. Adra, C.L. Aukim-Hastie, P.A. Townsend, Discovery of serum protein biomarkers for prostate cancer progression by proteomic analysis. *Cancer Genomics Proteomics* **2010**, *7*, 93.
23. C. Fania, I. Sogno, M. Vasso, E. Torretta, R. Leone, A. Bruno, P. Consonni, A. Albini, C. Gelfi. A PSA-guided approach for a better diagnosis of prostatic adenocarcinoma based on MALDI profiling and peptide identification *Clin Chim Acta* **2015**, *439*, 42.

24. C.-D. Calvano, A. Aresta, M. Iacovone, G.-E. De Benedetto, C.-G. Zambonin, M. Battaglia, P. Ditonno, M. Rutigliano, C. Bettocchi. Optimization of analytical and pre-analytical conditions for MALDI-TOF-MS human urine protein profiles. *J Pharm Biomed Anal* **2010**, *51*, 907.
25. X. Wang, J. Han, D.-B. Hardie, J. Yanga, C.-H. Borchersa. The use of matrix coating assisted by an electric field (MCAEF) to enhance mass spectrometric imaging of human prostate cancer biomarkers. *J Mass Spectrom* **2016**, *51*, 86.
26. B. Flatley, P. Malone, R. Cramer. MALDI mass spectrometry in prostate cancer biomarker discovery. *Biochim Biophys Acta* **2014**, *1844*, 940.
27. D. Bonnel, R. Longuespee, J. Franck, M. Roudbaraki, P. Gosset, R. Day, M. Salzet, I. Fournier. Multivariate analyses for biomarkers hunting and validation through on-tissue bottom-up or in-source decay in MALDI-MSI: application to prostate cancer. *Anal Bioanal Chem* **2011**, *401*,149.
28. K. Schwamborn, R.-C. Krieg, M. Reska, G. Jakse, R. Knuechel, A. Wellmann. Identifying prostate carcinoma by MALDI-Imaging *Int J Mol Med* **2007**, *20*, 155.
29. Y. Zheng, Y. Xu, B. Ye, J. Lei, M.-H. Weinstein, M.-P. O'Leary, J.-P. Richie, S.-C. Mok, B.-C. Liu. Prostate carcinoma tissue proteomics for biomarker discovery. *Cancer* **2003**, *98*, 2576.
30. Z.-I. Khamis, K.-A. Iczkowski, Z.-J. Sahab, Q.-X. Sang. Protein profiling of isolated leukocytes, myofibroblasts, epithelial, basal, and endothelial cells from normal, hyperplastic, cancerous, and inflammatory human prostate tissues. *J Cancer* **2010** *1* 70.
31. J.-D. Pallua, G. Schaefer, C. Seifarth, M. Becker, S. Meding, S. Rauser, A. Walch, M. Handler, M. Netzer, M. Popovscaia, M. Osl, C. Baumgartner, H. Lindner, L. Kremser, B. Sarg, G. Bartsch, C.-W. Huck, G.-K. Bonn, H. Klocker. MALDI-MS tissue imaging identification of biliverdin reductase B overexpression in prostate cancer. J Proteom **2013**, *91*, 500.
32. A.-Y. Liu, H. Zhang, C.-M. Sorensen, D.-L. Diamond. Analysis of prostate cancer by proteomics using tissue specimens. J Urol **2005**, *173*, 73.

33. S. Magdeldin, T. Yamamoto. Toward deciphering proteomes of formalin-fixed paraffin-embedded (FFPE) tissues. *Proteomics* **2012**, *12*, 1045.
34. H.-R. Aerni, D.-S. Cornett, R.-M. Caprioli. High throughput profiling of formalin-fixed paraffin embedded tissue using parallel electrophoresis and matrix-assisted laser desorption ionization mass spectrometry. *Anal Chem* **2009**, *81*, 7490.
35. D. Calligaris, R. Longuespée, D. Debois, D. Asakawa, A. Turtoi, V. Castronovo, A. Noël, V. Bertrand, M.-C. De Pauw-Gillet, E. De Pauw. Selected protein monitoring in histological sections by targeted MALDI-FTICR in-source decay imaging. *Anal Chem* **2013**, *85*, 2117.
36. C.-B. Fowler, D.-L. Evers, T.-J. O'Leary, J.-T. Mason. Antigen Retrieval Causes Protein Unfolding Evidence for a Linear Epitope Model of Recovered Immunoreactivity. *J Histochem Cytochem* **2011**, *59(4)*, 366.
37. L.-H. Cazares, D. Troyer, S. Mendrinos, R.-A. Lance, J.-O. Nyalwidhe, H.-A. Beydoun, M.-A. Clements, R.-R. Drake, O.-J. Semmes. Imaging mass spectrometry of a specific fragment of mitogen-activated protein kinase/extracellular signal-regulated kinase kinase kinase 2 discriminates cancer from uninvolved prostate tissue. *Clin Cancer Res* **2009**, *15*, 5541
38. M.-R. Groseclose, P.-P. Massion, P. Chaurand, R.-M. Caprioli. High-throughput proteomic analysis of formalin-fixed paraffin-embedded tissue microarrays using MALDI imaging mass spectrometry. *Proteomics* **2008**, *8*, 3715.
39. H.C. Diehl, B. Beine, J. Elm, D. Trede, M. Ahrens, M. Eisenacher, K. Marcus, H.E. Meyer, C. Henkel. The challenge of on-tissue digestion for MALDI MSI - A comparison of different protocols to improve imaging experiments. *Anal. Bioanal. Chem.* **2015**, *407*, 2223.
40. T. Goto, N. Terada, T. Inoue, T. Kobayashi, K. Nakayama, Y. Okada, T. Yoshikawa, Y. Miyazaki, U. Masayuki, N. Utsunomiya, Y. Makino, S. Sumiyoshi, T. Yamasaki, T. Kamba, O. Ogawa. Decreased Expression of Lysophosphatidylcholine (16:0/OH) in High Resolution Imaging Mass

Spectrometry Independently Predicts Biochemical Recurrence After Surgical Treatment for Prostate Cancer. *The Prostate* **2015**, *75*, 1821.

41. H. Wang, J.P. DeGnore, B.D. Kelly, J. True, K. Garsha, C. Bieniarz. A technique for relative quantitation of cancer biomarkers in formalin-fixed, paraffin embedded (FFPE) tissue using stable-isotope label based mass spectrometry imaging (SILMSI). *J Mass Spectrom* **2015**, *50*, 1088.
42. S. Steurer, C. Borkowski, S. Odinga, M. Buchholz, C. Koop, H. Huland, M. Becker, M. Witt, D. Trede, M. Omidi, O. Kraus, A.-S. Bahar, A.-S. Seddiqi, J.-M. Singer, M. Kwiatkowski, M. Trusch, R. Simon, M. Wurlitzer, S. Minner, T. Schlomm, G. Sauter, H. Schlüter. MALDI mass spectrometric imaging based identification of clinically relevant signals in prostate cancer using large-scale tissue microarrays. *Int J Cancer* **2013**, *133*(4), 920.
43. M. Ringnér. What is principal component analysis? *Nature Biotechnol* **2008**, *26(3)*, 303.
44. D. Calligaris, D.-R. Feldman, I. Norton, O. Olubiyi, A.-N. Changelian, R. Machaidze, M.L. Vestala, E.R. Laws, I.F. Dunn, S. Santagata, N.-Y.R. Agar. MALDI mass spectrometry imaging analysis of pituitary adenomas for near-real-time tumor delineation. *PNAS* **2015**, 112(32), 9978.
45. A. Cassese, S.-R. Ellis, N.-O. Potočnik, E. Burgermeister, M. Ebert, A. Walch, A.-M.J.M. van den Maagdenberg, L.-A. McDonnell, R.-M.A. Heeren, B. Balluf. Spatial Autocorrelation in Mass Spectrometry Imaging. *Anal Chem* **2016**, *88(11)*, 5871.
46. J.-M. Fonville, C. Carter, O. Cloarec, J.-K. Nicholson, J.-C. Lindon, J. Bunch, E. Holmes. Robust data processing and normalization strategy for MALDI mass spectrometric imaging. *Anal. Chem*. **2012**, *84(3)*, 1310.
47. A. Broersen, R. van Liere, A.-F.M. Altelaar, R.-M.A. Heeren, L.-A. McDonnell. Automated, Feature-Based Image Alignment for High-Resolution Imaging Mass Spectrometry of Large Biological Samples. *J Am Soc Mass Spectrom* **2008**, *19*, 823.

48. L. O'Brien, P.A. Hosick, K. John, D.E. Stec, T.D. Hinds. Biliverdin reductase isozymes in metabolism. *Trends Endocrinol Metabol* **2015**, *26(4)*, 212.
49. P.-M. Angel, R.-M. Caprioli. Matrix-Assisted Laser Desorption Ionization Imaging Mass Spectrometry: In Situ Molecular Mapping. *Biochemistry* **2013**, *52*, 3818.

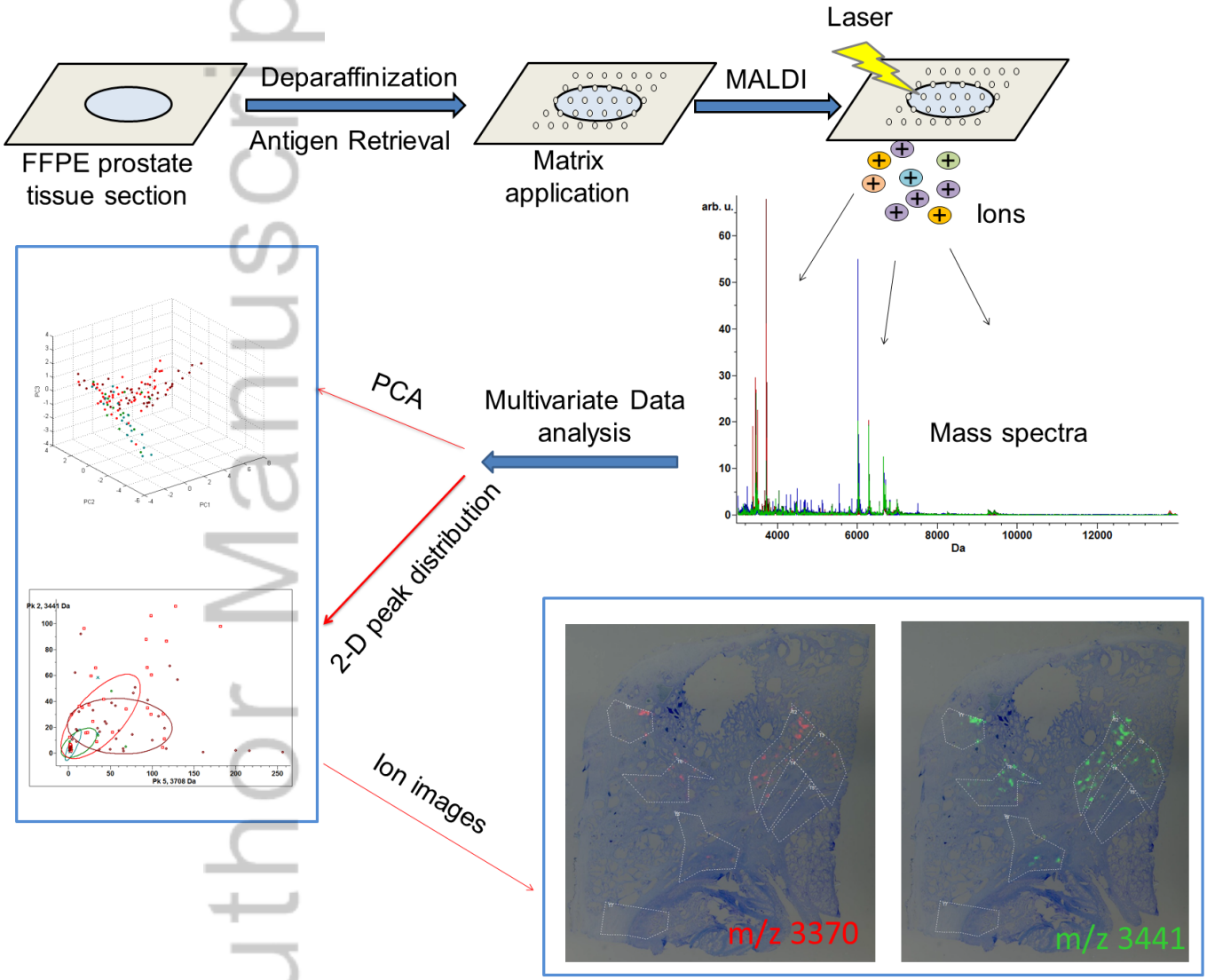

Table 1. Ion peaks of interest that account for the variation between tumor and non-tumor areas of prostate tissue

Case1							**Case 2**					
HIAR (TRIS buffer pH 9)				**HIAR (Citrate buffer pH 6)**			**HIAR (TRIS Buffer pH 9)**			**HIAR (Citrate Buffer pH 6)**		
Peak No	m/z	Dave[1]	p-value t-test ANOVA	m/z	Dave[1]	p-value t-test ANOVA	m/z	Dave[1]	p-value t-test ANOVA	m/z	Dave[1]	p-value t-test ANOVA
1	3707.76	53.42	< 0.000001	3440.47	130.18	< 0.000001	3440.47	130.18	< 0.000001	3440.62	113.15	< 0.000001
2	5999.34	42.63	< 0.000001	5999.28	41.54	< 0.000001	5999.28	41.54	< 0.000001	3369.93	52.25	< 0.000001
3	3440.78	24.43	< 0.000001	3369.52	32.35	< 0.000001	3369.52	32.35	< 0.000001	5999.37	44.65	< 0.000001
4	3484.7	16.32	< 0.000001	4815.05	23.55	< 0.000001	4815.05	23.55	< 0.000001	6013.34	16.81	< 0.000001
5	6013.31	16.2	< 0.000001	6013.32	15.96	< 0.000001	6013.32	15.96	< 0.000001	6027.9	8.79	< 0.000001
6	6271.2	14.66	< 0.000001	6027.97	8.35	< 0.000001	6027.97	8.35	< 0.000001	6684.52	7.39	< 0.000001
7	3369.84	13.97	< 0.000001	6684.43	7.33	< 0.000001	6684.43	7.33	< 0.000001	3454.37	5.61	0.138
8	3719.27	12.99	< 0.000001	3227.56	5.4	0.000267	3227.56	5.4	0.000267	3227.58	5.05	0.000535
9	6027.85	8.38	< 0.000001	4476.6	4.69	0.00000151	4476.6	4.69	0.00000151	4476.66	4.96	< 0.000001
10	3455	6.65	0.107	6656.5	4.22	0.00000547	6656.5	4.22	0.00000547	6656.47	4.25	0.00000545
11	6643.53	6.44	< 0.000001	3471.34	3.6	0.00102	3471.34	3.6	0.00102	4204.68	3.66	0.00000192
12	6283.02	5.76	< 0.000001	6041.9	3.1	< 0.000001	6041.9	3.1	< 0.000001	6042.13	3.27	< 0.000001
13	6684.43	4.88	2.39E-06	6643.89	3.06	0.00000969	6643.89	3.06	0.00000969	6643.98	3.17	0.00000711
14	4476.47	4.36	2.94E-06	6799.02	2.94	< 0.000001	6799.02	2.94	< 0.000001	3470.98	2.98	0.00422
15	6798.66	2.2	0.0000025	3454.33	2.85	0.441	3454.33	2.85	0.441	6799.13	2.76	< 0.000001
16	6698.23	1.1	0.00116	6698.42	2.64	< 0.000001	6698.42	2.64	< 0.000001	4836.57	2.67	0.000537
17	13795.6	0.67	< 0.000001	5983.47	2.5	0.00000846	5983.47	2.5	0.00000846	6698.44	2.65	< 0.000001
18	6656.26	0.41	0.619	6271.33	2.37	0.00629	6271.33	2.37	0.00629	6271.57	2.63	0.00304
19	6669.94	0.34	0.181	4836.65	1.79	0.0108	4836.65	1.79	0.0108	5983.75	2.49	0.0000082
20	9403.08	0.07	0.624	6055.12	1.78	< 0.000001	6055.12	1.78	< 0.000001	4673.89	2.43	0.00571

[1] Difference between the maximum and minimum average peak area of all classes; grey regions in table represents ion peaks with p values > 0.05